Mixed-Signal IC With Pulse Width ModulationWireless Telemetry for Implantable CardiacPacemakers in 0.18-µm CMOS

Rezaeiyan, Yasser; Zamani, Milad; Shoaei, Omid; Serdijn, Wouter A.

DOI
10.1109/TBCAS.2018.2819021

Publication date
2018

Document Version
Accepted author manuscript

Published in
IEEE Transactions on Biomedical Circuits and Systems

Mixed-Signal IC with Pulse Width Modulation Wireless Telemetry for Implantable Cardiac Pacemakers in 0.18 µm CMOS

Yasser Rezaeiyan, Milad Zamani, *Student Member, IEEE*, Omid Shoaei, *Member, IEEE* and Wouter A. Serdijn, *Fellow, IEEE*

***Abstract*— A low power mixed-signal IC for implantable pacemakers is presented. The proposed system features 3 independent intra-cardiac signal readout channels with pulse width modulated outputs. Also, the proposed system is capable of measuring the amplitude and phase of the bio-impedance with pulse width modulated outputs for use in rate adaptive pacemakers. Moreover, a stimulation system is embedded, offering 16 different amplitudes from 1 to 7.8 V. A backscattering transmitter transfers the output signals outside the body with very little power consumption. The proposed low power mixed-signal IC is fabricated in a 0.18 µm HV CMOS process and occupies 2.38 mm^2. The bio-potential channels extract the heart signals with 9.2 effective number of bits (ENOB) and the bio-impedance channels measure the amplitude and phase of the heart impedance with 1.35 Ω_{rms} accuracy. The complete IC consumes only 4.2 µA from a 1 V power supply.**

***Index Terms*— ASIC, bio-impedance, bio-potential amplifier, intra-cardiac signal, active implantable medical device, cardiac pacemaker, wireless communication, low power.**

I. Introduction

THE increasing number of patients using cardiac pacing devices (pacemakers) make these microsystems the most common active implantable medical devices nowadays on the market. Implantable pacemakers improve the quality of life and give the patients near normal life functionality [1]. Several factors, however, make the design of a cardiac pacemaker a challenging task. These factors are the required small form factor, the very low power consumption, the pacemaker's rate adaptive feature and its data transmission [2, 3, 13].

Pacemakers are highly energy constrained and should offer years of operation on a single battery to avoid repeated surgery, which demands the use of low power on-chip circuitry, including input readout channels, digital control, data transceiver, pulse generator and auxiliary circuitry [4].

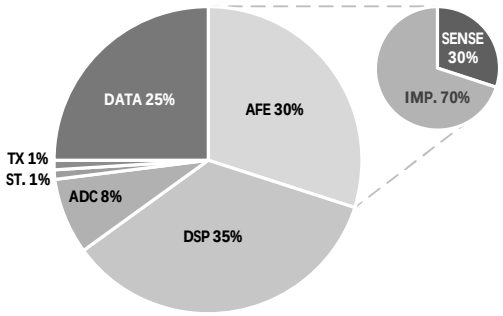

Fig. 1. Typical power consumption chart of fundamental pacemaker blocks [2], [3].

Pacemakers consist of several blocks that have different active times. For example, the stimulator block stimulates the heart only in case of arrhythmias; the sense amplifiers continuously monitor the natural activity of the heart chambers; the bio-impedance measurement unit also measures continuously, albeit at a lower rate; finally, the wireless transmitter transmits recorded data on demand and at a higher data rate. Digital signal processing, analog to digital conversion (ADC), data storage and coding and modulation for wireless communication usually require the majority of the available power in biomedical devices (Fig. 1) [2], [23]. The power consumption can be further reduced by taking a new system-level design approach that eliminates the need of internal digital processing, ADC, data storage, coding and modulation and ensures maximum functionality. Backscattering is a data transmission method that offers such a very low power consumption [5]. Backscattering is also good from a security perspective, as repeated attacks/requests will not drain the battery.

The principles of measuring the bio-impedance and the intra-cardiac electrogram (IECG) for cardiac pacemakers and how to convert these into pulse-width modulated (PWM) output signals are presented by the authors in [20] and [21], respectively. From these PWM output signals, the bio-impedance and IECG can be extracted. In a pacemaker, the information to be extracted from the IECG signal is whether the heart chamber has contracted naturally, i.e., without an electrical stimulus from the pacemaker. This boils down to

Yasser Rezaeiyan and Milad Zamani are with Bio-Integrated Systems Lab, School of Electrical and Computer Engineering, University of Tehran, Tehran, Iran. (E-mail: yrezaeiyan@ut.ac.ir, miladzamani@ut.ac.ir).

Omid Shoaei is with Nano-Electronic Center of Excellence and Bio-Integrated Systems Lab, School of Electrical and Computer Engineering, University of Tehran, Tehran 1439957131, Iran. (E-mail: oshoaei@ut.ac.ir).

Wouter A. Serdijn is with the Section Bio-Electronics, Faculty of Electrical Engineering, Mathematics and Computer Science, Delft University of Technology, 2628 CD Delft, The Netherlands (E-mail: w.a.serdijn@tudelft.nl).

(Yasser Rezaeiyan and Milad Zamani contributed equally to this work)

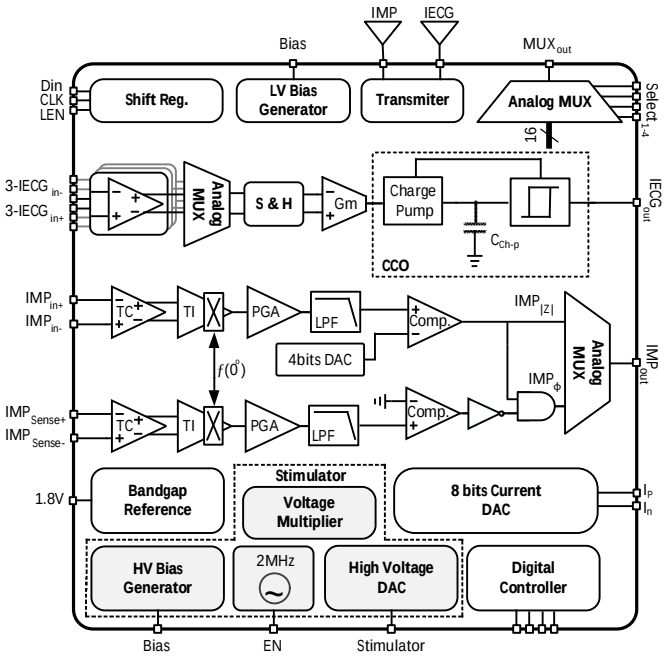

Fig. 2. ASIC Architecture.

checking for the presence of an R- or a P-wave in the IECG signal [29]. From the bio-impedance signal, in so-called rate-responsive pacemakers, only the breathing rate has to be extracted, which is an indication of the pacing rate of the pacemaker. For this, the course information present in the magnitude of the bio-impedance suffices [31-33]. Both types of information can be readily extracted from the PWM output signals by means of relatively simple, and thereby low-power, circuitry that can be incorporated in the pacemaker itself.

For monitoring and diagnostic purposes, however, analysis of the entire cardiac IECG signal and the magnitude and phase of the bio-impedance signal might be useful. This signal analysis is more computationally demanding [30] and, hence, is preferably done outside the body, where, compared to the pacemaker, there is much more electrical power and space available, provided, of course, that the wireless communication from the pacemaker to the outside can be done in a low-power fashion. The PWM signals that represent the IECG and bio-impedance signals are suitable for such a low-power wireless link.

In this paper, a novel approach to the design of a cardiac pacemaker is presented that employs this way of converting the signals and eliminates the need for ADCs and data storage by generating a proper output signal for a low power wireless data link employing backscattering. The proposed system provides complete pacemaker functionality. The essential operation of the bio-impedance and IECG front-end will be briefly explained again in this paper for a proper understanding of the complete system.

As an embodiment of the above system-level approach, in this paper, an Application-Specific Integrated Circuit (ASIC) is presented with some unique features (Fig. 2):

1) 3 channels that provide the IECG bio-potential readout for a 3-lead pacemaker. The bio-potential readout system features voltage to frequency conversion. The output of these channels are frequency-shift-keying and pulse-width modulated (FSK-PWM), which provides data transmission with very little power consumption [14].

2) A bio-impedance measurement readout channel with amplitude and phase branches that monitors the biophysical properties. This system benefits from a semi-ramp signal instead of a pure analog sinusoidal signal, the former of which can be synthesized in a less power-hungry fashion. The output of this channel is PWM for both amplitude and phase, which yields a power efficient method for signal transmission.

3) A stimulator that generates pulses with programmable voltage amplitude and pulse duration. The stimulator uses 1.8 V for voltage multiplication and 1 V as the reference input to stimulate the heart muscle with 16 different pulse amplitude levels ranging from 1 to 7.8 V.

4) A multichannel transmission system that benefits from back-scattering and uses frequency-division multiple access (FDMA) via two inductive coils. Since the output signals of the above two channels are PWM, the modulation is done using switching circuitry by means of on-off keying (OOK).

This paper is organized as follows: Section II describes the ASIC architecture and its sub-blocks. Section III presents the principle of the proposed bio-potential measurement system. Section IV discusses the bio-impedance measurement method and the current injection mechanism. Section V discusses the stimulator system blocks and requirements. Section VI presents the details of the data transmission method. Section VII shows the measurement results and system functionality, Section VIII provides recommendations for future work and, finally, Section IX concludes the paper.

II. ASIC ARCHITECTURE

The ASIC (Fig. 2) consists of four major building blocks: 1) a sense amplifier, comprising three readout channels for acquiring IECG signals, 2) phase and amplitude bio-impedance readout channels for extracting intra-cardiac bio-impedance, 3) a high voltage output pulse generator to stimulate the heart muscle, and 4) a transmitter for transmitting the sense channel and the bio-impedance channel outputs. In addition to these major building blocks, the ASIC also includes a band-gap voltage reference, an 8 bits current digital to analog converter (current DAC), a digital controller, a 16 bits shift register, a 16-1 multiplexer (MUX), a 2 MHz oscillator, a bias generator for the high voltage (HV) blocks and a bias generator for the low voltage (LV) blocks. The LV bias generator block provides the necessary biasing voltage and current for the low voltage blocks and the HV bias generator provides the necessary biasing voltage and current for the high voltage blocks in the stimulator. By separating the low voltage and high voltage bias generators, the low voltage blocks (bio-potential front-end, bio-impedance front-end and transmitter) and the high voltage block (stimulator) are working together with sufficient isolation.

The operation of the ASIC for each major building block can be described as follows: The IECG readout channel extracts the bio-potential signal and converts the voltage to the frequency of an FSK-PWM signal. This FSK-PWM output signal is ready to be transmitted without the need for an ADC

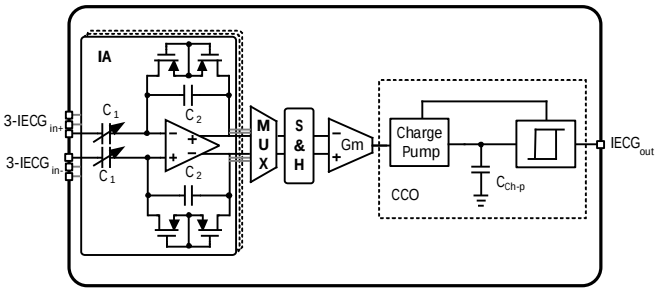

Fig. 3. Bio-potential measurement system architecture.

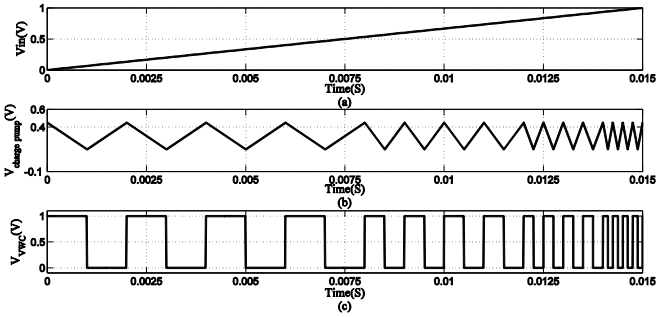

Fig. 4. Voltage to frequency conversion concept. a) The input voltage is a ramp waveform. b) The charge-pump capacitor voltage slope changes proportionally. Thus, the Schmitt trigger output is a FSK-PWM (c).

and digital modulation. In addition, an 8 bits current DAC drives the electrode-tissue interface with a semi-ramp signal. The bio-impedance readout channel continuously monitors the motion induced signal artifacts on this semi-ramp signal and also produces a PWM signal. This PWM output signal is ready to be transmitted via switching circuitry generating an OOK pattern without the need for an ADC and digital modulation. Moreover, a high voltage output pulse generator stimulates the heart muscle (for example during cardiac arrhythmias). Finally, the transmitter block prepares the outputs of the sense and bio-impedance channels for transmission via back-scattering.

III. BIO-POTENTIAL MEASUREMENT

The key requirements of a pacemaker are the extraction, analysis and wireless transmission of IECG signals with very low power consumption [3].

As the digital and radio blocks are the main source of power consumption [2], it is important to reduce the battery drainage while maintaining reliable communication. Conventional bio-potential systems use the digital output from an ADC for digital modulation, which is a power hungry operation. The dominant power consumption part can be removed if the digital signal processing is done externally and the output signal of the front-end is ready for transmission without any further manipulation and processing. The proposed bio-potential front-end [20] benefits from voltage to frequency (or time) conversion which is very low power, precise, accurate, simple and can be transmitted using backscattering [6].

Fig. 3 shows the architecture of the bio-potential measurement system. The proposed implementation employs an instrumentation amplifier (IA) with capacitive coupling and

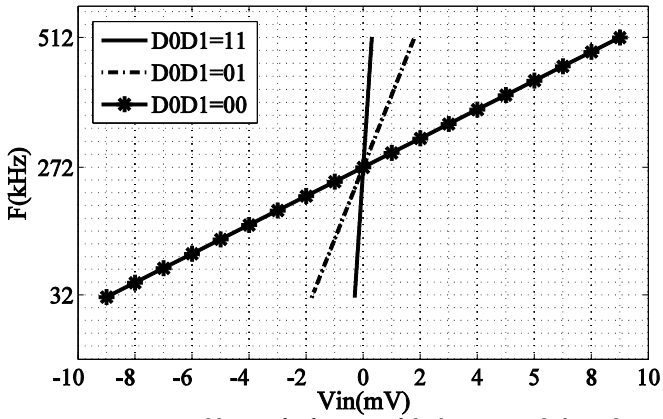

Fig. 5. Programmable transfer function of the bio-potential channel.

TABLE I
BIO-POTENTIAL DESIGN SPECIFICATION AND MEASUREMENT SUMMARY

	Target Specification	Measurement
Operating voltage	1V	1V
Gain	14-28-44 dB	14-28.5-44 dB
BW	10 – 120 Hz	8 – 120 Hz
Input Dynamic Range	±50µVpp/ ±10mVpp	±50µVpp/ ±9mVpp
CMRR	>90 dB	>90 dB
Input Referred Noise @ 44dB Gain	< 5 µVpp Over 150Hz	$2\mu V_{rms}$ Over 150Hz
Output Freq. Range	Up to 512 kHz	Up to 512 kHz
Power Consumption per channel	< 0.5 µW	0.5 µW

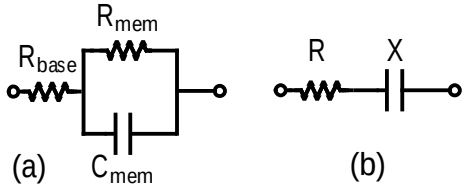

Fig. 6. a. Three-element bio-impedance model of cardiac tissue. b. Simplified equivalent circuit.

feedback to eliminate the input offset and also to benefit from programmability with three different gain settings (equal to C_1/C_2) to increase the input dynamic range. The input referred noise of the IA is the dominant noise source of the overall bio-potential channel. The total noise of the IA is related to the noise of the operational transconductance amplifier (OTA) and also the loop gain [7], [8]. The IA amplifies the intrinsic cardiac voltage and provides three different gain settings (14-28-44 dB). A sample of the input voltage is held in a sample and hold block in front of the transconductance amplifier (Gm) block. The differential output voltage of the IA is transformed into a current by means of a trans-conductance amplifier with a G_m of 1 µS. The output current of the trans-conductance amplifier feeds a charge pump that produces a saw-tooth waveform by injecting the current into a capacitor via two controlled switches. These switches control the time interval of the charge pump that sinks or sources the output capacitance. A Schmitt trigger is responsible for comparing the saw-tooth waveform with a high voltage reference and a low voltage reference. The combination of a charge-pump and a Schmitt trigger makes a current controlled oscillator (CCO) function. The output of the Schmitt trigger comparator provides the switching signal of the charge pump as well as

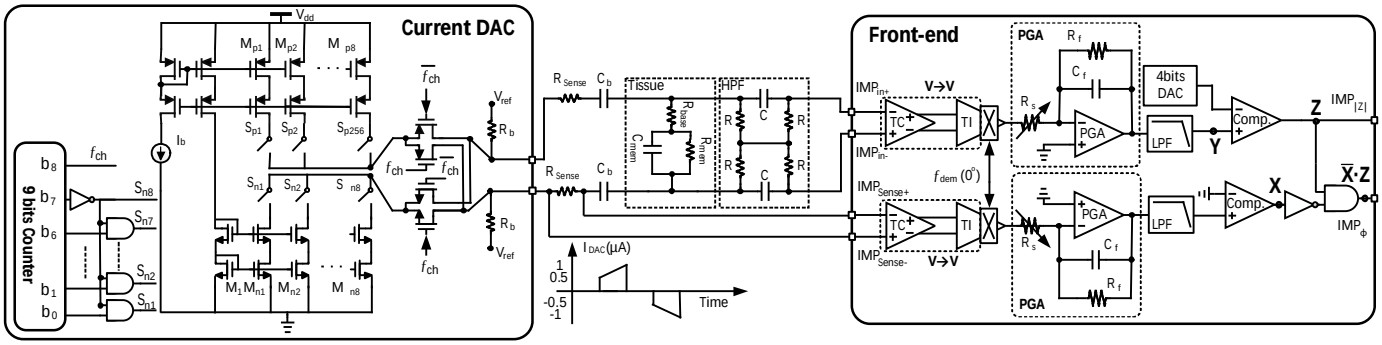

Fig. 7. Bio-impedance measurement system architecture [21].

the output of the bio-potential system [20].

Fig. 4 shows the voltage to frequency conversion method. As the input voltage goes higher, the output current of the trans-conductance amplifier increases. Hence, the output current of the G_m block charges and discharges the output capacitor of the charge pump faster and, consequently, the Schmitt trigger produces a PWM signal with a higher frequency. Counting the number of pulses as a function of time, the input voltage can be reconstructed from the output PWM signal.

The momentary output PWM signal frequency can be written as:

$$f_{out} = f_0 + \frac{A_{IA} G_m}{2 C_{ch.p} V_{Hys}} V_{in}(t), \quad (1)$$

where A_{IA} is the gain of the input instrumentation amplifier, G_m is the gain of the trans-conductance amplifier, $C_{ch.p}$ is the output capacitance of the charge pump, f_0 is the mean frequency of the output signal, which is related to the dc current of the G_m and is necessary for reading negative input voltages, and V_{Hys} is the hysteresis voltage of the Schmitt trigger. The output frequency range can be adapted to the instrumentation amplifier input signal range by adjusting its programmable gain.

Fig. 5 shows the transfer function of the bio-potential channel. To increase the readout dynamic range, 3 different gain settings are utilized to change the slope of the output frequency according to (1). The output frequency of each range is bounded to 32-512 kHz to decrease the power consumption and maintain enough resolution and linearity. The reconstruction of the input signal from the output frequency is based on (1) by counting the zero-crossings of the output PWM signal in a specific time interval. The reconstruction process is the averaging of the frequency in each interval. Using a moving average technique one can show that the reconstructed transfer function is a low pass filter, the cut-off frequency of which depends on the counting time interval of the zero crossing events. Table I shows the key specifications of the system that meets the IECG requirements [20].

IV. BIO-IMPEDANCE MEASUREMENT

Measurement of the electrical bio-impedance of organs and heart tissue has become the most suitable method for monitoring their biophysical properties [3], [9]. Various methods are used to extract the real and imaginary parts (i.e., the Cartesian coordinates) of the (complex) bio-impedance [9]. Another promising alternative method is measuring the magnitude and the phase (i.e., the polar coordinates) of the (complex) bio-impedance [10].

For electrical bio-impedance measurement, an excitation current is injected into the tissue with a bipolar lead. Fig. 6a shows a three-element model of cardiac tissue with two resistances and one capacitance, of which the parallel resistance and capacitance are related to the cell membrane characteristics. Fig. 6b shows a simplified equivalent circuit of the tissue with ideal components. In reality, the resistance and capacitance depend on the frequency. This equivalent model as a complex impedance $Z=R+jX$ is valid as an approximation within a limited frequency range around the measurement frequency [9], [16]. The real and imaginary parts of the bio-impedance provide the following useful information [9], [17]: 1) information on the fast bio-impedance fluctuations due to the beating of the heart and 2) information of the slow bio-impedance fluctuations due to the movement of the chest due to respiration.

Fig. 7 shows the architecture of the impedance measurement system [21]. The proposed implementation employs an 8 bits current DAC to inject current into the tissue. The current injection circuit must meet specific features such as low-power operation, frequency range and amplitude in agreement with the IEC60601-1 medical standard [18]. We propose a semi-ramp waveform at 2 kHz as the tissue injection current with an increasing magnitude (500 nA-1 µA). The 2kHz chopping signal, f_{ch}, is derived from the 1 MHz clock signal by means of a (divide by 512) frequency divider.

To calculate the impedance at a single frequency, obviously and by definition, a pure sinusoidal source is needed. Using other signals causes errors in the bio-impedance measurement. However, sinusoidal oscillators tend to be power hungry [3], [26-27]. On the other hand, using a square signal instead of a sinusoid causes a significant error in the impedance measurement [9], [28]. A three-level injection signal is as easy

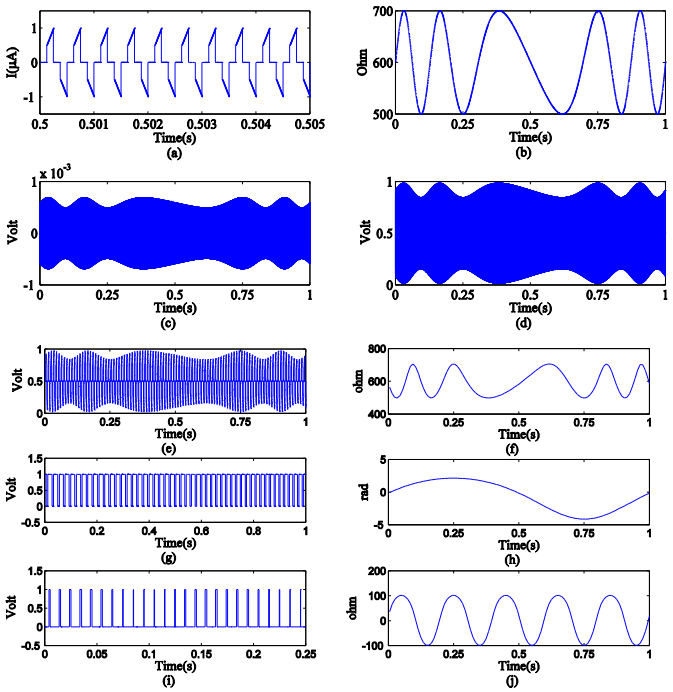

Fig. 8. Bio-impedance system level simulation [21]. a) semi-ramp DAC output signal. b) Heart tissue bio-impedance with varying magnitude and phase. c) The voltage produced after current injection into the heart tissue. d) The output signal of the mixer. e) The comparator input signal. f) Reconstructed impedance of the tissue impedance. g) The PWM output of the phase channel. h) Reconstructed phase of the heart tissue. i) The PWM output of the magnitude channel. j) Reconstructed magnitude of the heart tissue impedance.

to generate as a square signal and resembles a sinusoidal signal better (in terms of harmonics) and consumes even less power [9]. Our system takes this idea one step further and uses a semi-ramp signal. Using a semi-ramp signal results in almost the same accuracy as when using a three-level signal and allows for the generation of a PWM output signal directly, without the need for an ADC, which is the main advantage of the proposed system.

Each bio-impedance channel employs a cascade of a trans-conductance (TC) amplifier and a trans-impedance (TI) amplifier with an internal mixer driven by the demodulation frequency (f_{dem}) to extract the amplitude and phase, respectively. Each channel then continues with a programmable gain amplifier (PGA) to increase the input dynamic range. Also, in each channel, a 2-stage switched capacitor low-pass filter is utilized. Finally, two comparators compare the voltage of each branch with the reference voltage produced by a 4-bit voltage DAC and ground, respectively.

Fig. 8 shows the signals at different nodes of the magnitude and phase channels extracted from a system level simulation in MATLAB [21]. The injected current is a 2-kHz semi-ramp shape current which has positive, zero and negative parts (Fig. 8a). The time varying bio-impedance magnitude (500 Ω to 700 Ω) and phase (-π radiance to π radiance) (Fig. 8b) modulate the amplitude and phase of the semi-ramp signal at 2kHz (Fig. 8c). The magnitude readout channel employs an instrumentation amplifier (IA) to provide the required voltage gain (Fig. 8d). After mixing with the clock signal, the filtered

TABLE II
BIO-IMPEDANCE DESIGN SPECIFICATION AND MEASUREMENT SUMMARY

	Target Specification	Measurement
Operating voltage	1V	1V
Gain	40-49-55-62 dB	39-48.5-55.5-62 dB
BW	0.5-10 Hz	0.1-10 Hz
Input Dynamic Range	3.3 mV	3.3 mV
Input referred Noise @ 40dB Gain	<2 μV_{rms}	0.7 μV_{rms}
CMRR	>90 dB	95 dB
THD	1%@ <1 kΩ @10 Hz	1%@ <1 kΩ @10 Hz
Injection Current	0.5-1 μA	0.5-1μA
Output Freq. Range	Up to 100 Hz	Up to 100 Hz
Tissue Impedance Range	100-3000 Ω	100-3300 Ω
Power Consumption	<2 μW	1.55 μW

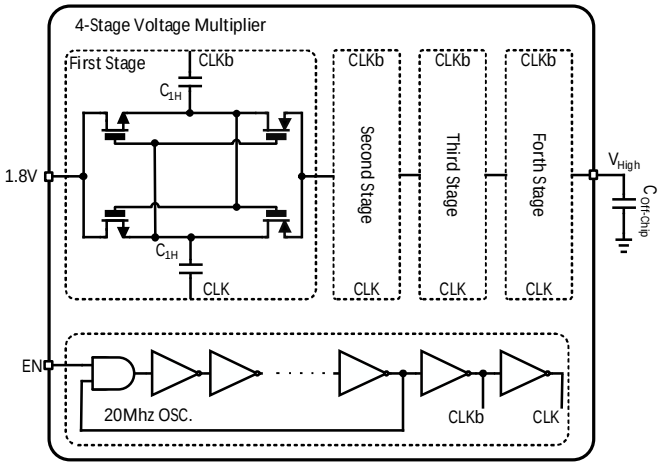

Fig. 9. 4-stage voltage multiplier. An internal ring oscillator produces the required clock for the multiplier stages. The output off-chip capacitor is a source of power for the other stimulator parts.

output voltage (Fig. 8e) benefits from the ramp shape and easily provides a PWM signal after comparison with the reference voltage. Fig. 8f is the reconstructed impedance of the tissue. The pulse widths of the phase (Fig. 8g) and the amplitude (Fig. 8i) channels are directly related to the bio-impedance phase and amplitude, respectively. The *Z* signal is the output of the magnitude channel. The magnitude of the impedance can be extracted from the pulse width of the output PWM signal (Fig. 8j). Thus, the $\overline{x}.z$ waveform is the difference of the reference signal and the PWM signal of the magnitude channel. The phase data can be reconstructed from the pulse width of this signal exactly (Fig. 8h) [21].

Finally, the analog MUX working at 2 MHz is used for multiplexing both phase and magnitude channels to transmit their data simultaneously. See Fig. 1. Table II shows the key specifications of the system that meets the bio-impedance measurement requirements [21].

V. STIMULATOR SYSTEM

Pacemakers monitor the heart rate and rhythm and provide electrical stimulation whenever the heart fails to produce a

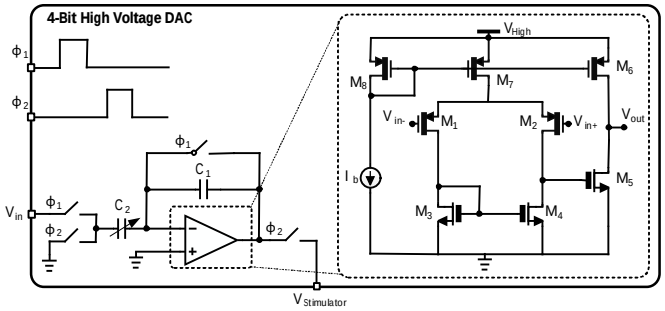

Fig. 10. 4-bit high-voltage DAC. 4 bits adjust the output voltage of the DAC with 16 different amplitudes. The pulse width of output voltage is set by 2 switching signals from the controller.

heartbeat itself. To stimulate the heart tissue artificially, a high voltage pulse is delivered through the lead [12]. The amplitude and pulse width of the stimulating signal must be programmable. The amplitude and the pulse width are set by the physician depending on the patient physical condition, tissue condition and the lead connection.

The primary voltage source of the system is the battery, which delivers 1.8 V at its end-of-life. Therefore, a voltage multiplier is required to produce the required higher voltages. The pacing can be from 1 up to 8 volt [1]. Fig. 9 shows the high voltage multiplier. From a 1.8 V supply, only 4 stages are needed to generate the required output voltage, which is the supply voltage of the high-voltage digital to analog converter (HV-DAC). This helps to improve the efficiency of voltage multiplier. Its basic stage is a two-phase charge-pump voltage doubler [11]. During the first clock phase, C_{0H} charges to the input voltage and during the second cycle cycle, C_{1H} charges to the input voltage. The required clock phases are generated by a ring oscillator working at around 2 MHz. The output voltage of each stage is the input voltage of that stage plus the clock voltage, which is the same as the first stage input voltage. Using 4 doubler stages and high voltage transistors to avoid breakdown, the output voltage can reach 8 V. The output voltage equals:

$$V_{out} = V_{in} + 4\Delta V = V_{in} + 4V_{clk} \cdot \frac{C}{C + C_{par}} - 4R_{Out} I_{Out}, \qquad (2)$$

where C is the intermediate capacitance in each section that is connected to the clock, V_{in} is the input reference voltage, C_{par} is the parasitic capacitance of the intermediate capacitors (bottom plate parasitic capacitance and transistor parasitic capacitance), V_{clk} is the clock voltage and R_{out} is the voltage multiplier load resistance.

Output current I_{out} of the voltage multiplier is only delivered during pacing. Thus, in the multiplication phase this output current is zero. The transistors of the voltage multiplier and the driver stage must be carefully dimensioned so that the power transfer in each cycle is efficient. When the pacemaker is not pacing, the high voltage DAC is off. However, the high voltage multiplier is working to provide a fast settling time. Not being loaded by the high voltage DAC, its only power loss is switching loss, which is negligible.

Fig. 9 shows the 4-stage voltage multiplier with its internal oscillator. To provide the consecutive charging and discharging operation of the capacitances in the voltage multiplier, an on-chip ring oscillator generates a high frequency clock to alleviate the requirement of big capacitors at the internal nodes. The multiplier starts producing the high voltage after enabling the ring oscillator. An off-chip capacitor (100 nF) is selected based on the current requirement of the stimulator.

TABLE III
TARGET AND MEASUREMENT SPECIFICATIONS OF THE STIMULATOR SYSTEM

	Target Specification	Measurement
Operating voltage	1.8 V	1.8 V
Pulse amplitude	1-8 V	1-7.8 V
Voltage DAC r_{out}	1 kΩ	1 kΩ
Max. Power efficiency	>50%	55%
Clock frequency	2 MHz	2 MHz
Settling time	<30 µs	35 µs
Gain error	<10%	3%
Number of bits	4	4

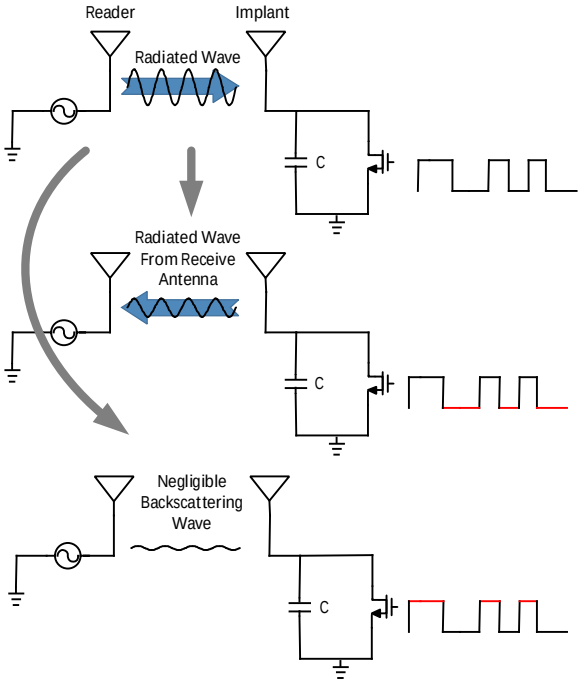

Fig. 11. Backscattering communication with a PWM signal as input to the switching circuitry.

Fig. 10 shows the 4-bits high-voltage DAC to stimulate the heart muscle. During the pre-charge phase, all ϕ_1 switches are closed and the input voltage is stored on C_2. During the output phase all ϕ_2 switches are closed to form a feedback loop. The high voltage opamp provides a gain of C_2/C_1. C_2 can be adjusted by means of 4 switches and provides 16 different output voltages for stimulation. The input voltage of the high voltage DAC is 1 V and it provides an output voltage ranging from 1 to 7.8 V. The duration of the stimulation can be set by output switch signal ϕ_2.

In order to stimulate effectively, the high voltage stimulator needs to stimulate the heart only with a very short duty cycle. In addition, in case of natural pacing, the stimulator is off. Besides these specifications, the programmability of the amplitude and the pulse width of the stimulation signal are the

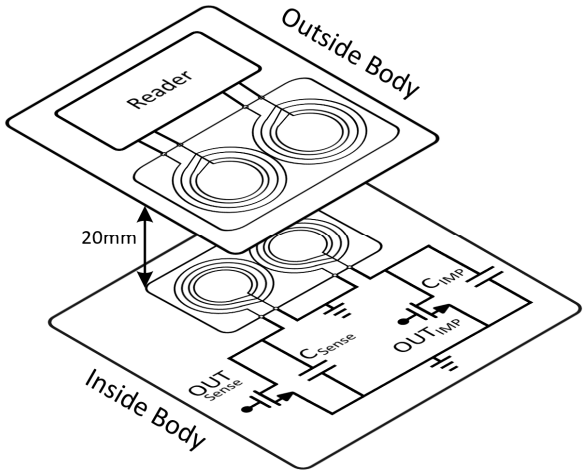

Fig. 12. Two inductive data links. A backscatterer is used inside the body with two coils operating at different frequencies. The reader is outside the body with two coils operating at the same frequencies as the backscatterer

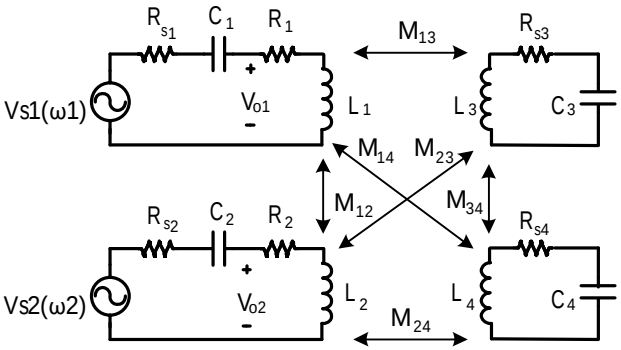

Fig. 13. Electrical model of the four inductive coils that are used in the two data links.

main considerations [1]. A summary of the pulse generator parameters is given in Table III.

VI. Data Transmission

A backscatter radio link communicates by modulating the scattered electromagnetic wave incident from the reader. The scattered wave is modulated by changing the electrical impedance presented to the antenna (Fig. 11) [14]. A backscatterer does not use a radio transmitter. It is one of the best solutions for minimizing the power consumption of the pacemaker that is implanted inside the body with a limited power source. The use of a backscatter link means that the modulation switching circuitry in the backscatterer only needs to operate at modest frequencies comparable to the data, not the carrier frequency [6].

Fig. 12 shows the configuration of the implant and the reader that is outside of the body. Since the output of the sense channel and the multiplexed bio-impedance channels are both PWM signals, two different modulation switching circuits are used to transmit the data at different frequencies.

Fig. 13 illustrates the model of the inductive data link with two spiral inductors inside the body and two spiral inductors outside of the body. L_1 and L_2 are related to the reader inductors and L_3 and L_4 are related to the implant. L_3 reflects the transmitted power of V_{S1} (the power source of the first transmitter) and L_4 reflects the transmitted power of V_{S2} (the power source of the second transmitter). For simplicity the effect of the reflected power from the undesired backscatterer is ignored (which is expected to be low as it is at a different frequency). With this assumption the transfer function that shows the relation of this reflected power can be written as:

$$\begin{aligned} V_{o1} &= V_{s1}(\omega_1)H_{11}(\omega_1) + V_{s2}(\omega_2)H_{12}(\omega_2) \\ V_{o2} &= V_{s1}(\omega_1)H_{21}(\omega_1) + V_{s2}(\omega_2)H_{22}(\omega_2) \end{aligned} \tag{3}$$

H_{11} represents the reflected power from the backscatterer when the related source transmits the power. Also, H_{22} is the transfer function of the other data link.

The transfer function of the reflected power of the first data link is:

$$\begin{aligned} H_{11} &= 1-(Rs_1+1/(C_1 j\omega_1))/((Z_4 M_{23}{}^2\omega_1{}^2 \\ &+M_{23}M_{24}M_{34}\omega_1{}^3(-2i)+Z_3 M_{24}{}^2\omega_1{}^2 \\ &+Z_2 M_{34}{}^2\omega_1{}^2+Z_2Z_3Z_4)/A(\omega_1)) \end{aligned} \tag{4}$$

The transfer function of the other data link is

$$\begin{aligned} H_{12} &= (Rs_1+1/(C_1 j\omega_2))\times \\ &\times((M_{13}M_{24}M_{34}\omega_2{}^3+M_{13}M_{23}\omega_2{}^2Z_4 i \\ &+M_{14}M_{24}\omega_2{}^2Z_3 i-M_{12}\omega_2 Z_3Z_4-M_{12}M_{34}{}^2\omega_2{}^3, \\ &+M_{14}M_{23}M_{34}\omega_2{}^3)/A(\omega_2)) \end{aligned} \tag{5}$$

where $A(\omega_1)$, mutual inductance M and coupling factor K are equal to:

$$\begin{aligned} &\mathrm{A}(\omega_1)= \\ &\left(\begin{matrix}-2M_{12}M_{13}M_{24}M_{34}-2M_{12}M_{14}M_{23}M_{34} \\ +M_{13}{}^2M_{24}{}^2-2M_{13}M_{14}M_{23}M_{24}+M_{14}{}^2M_{23}{}^2\end{matrix}\right)\omega_1{}^4+ \\ &\left(\begin{matrix}Z_4M_{12}M_{13}M_{23}(-2i)+Z_3M_{12}M_{14}M_{24}(-2i) \\ +Z_2M_{13}M_{14}M_{34}(-2i)+Z_1M_{23}M_{24}M_{34}(-2i)\end{matrix}\right)\omega_1{}^3+ \\ &\left(\begin{matrix}Z_3Z_4M_{12}{}^2+Z_2Z_4M_{13}{}^2+Z_2Z_3M_{14}{}^2+Z_1Z_4M_{23}{}^2 \\ +Z_1Z_3M_{24}{}^2+Z_1Z_2M_{34}{}^2\end{matrix}\right)\omega_1{}^2+ \\ &\mathrm{Z}_1\mathrm{Z}_2\mathrm{Z}_3\mathrm{Z}_4 \\ &M \cong \frac{\mu_0 N_T d_T^2 N_R d_R^2 \pi}{2\sqrt{(d_R^2+Z^2)^3}} \\ &K = \frac{a^2b^2}{\sqrt{ab}(\sqrt{a^2+Z^2})^3}, \end{aligned} \tag{6}$$

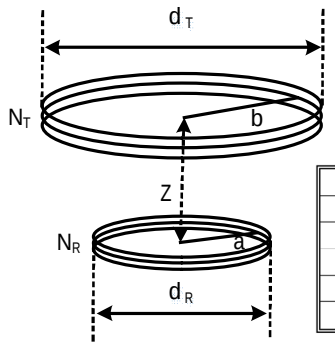

	IECG	Bio-imp.
b	13mm	10mm
N_T	2	2
Z	20mm	20mm
a	8mm	6mm
N_R	8	8

Fig. 14. External (reader) and internal (backscatterer) coils with their dimensions.

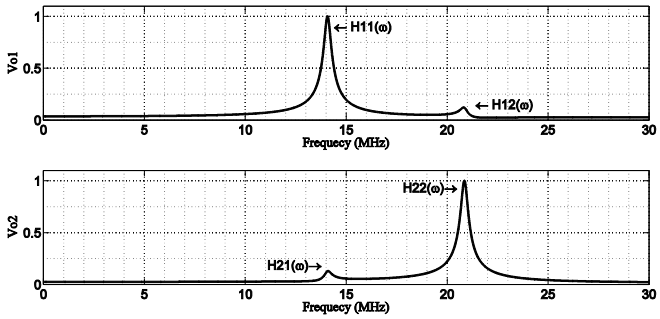

Fig. 15. Simulated normalized voltage of two data links related to bio-potential and bio-impedance channels. The output of each voltage is the sum of two transfer functions related to the power of reader transmitters. The power of bio-potential reader is hardly seen by the bio-impedance reader and vice versa in their frequency.

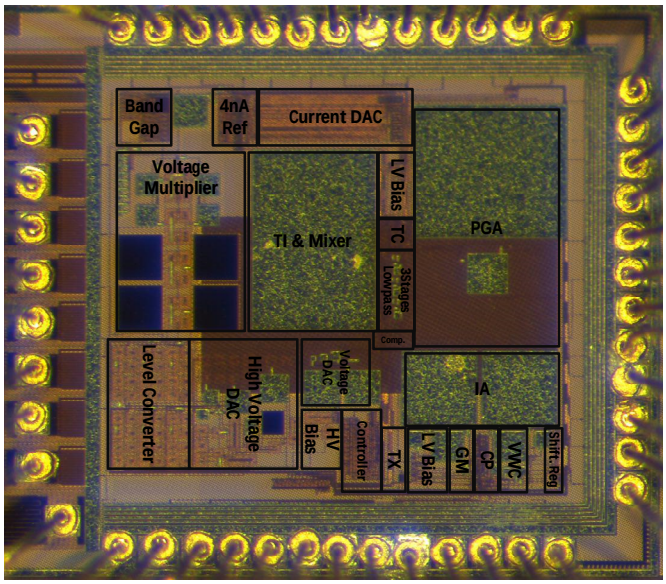

Fig. 16. ASIC chip micrograph.

where *a*, *b*, *Z*, d_R and d_T are the coil parameters (Fig. 14). Also, H_{22} and H_{21} are calculated with the same method.

Fig. 14 shows the two coils of the backscatterer and the reader with their dimensions. The maximum distance between the two coils is assumed to be 20 mm [13, 19].

Fig. 15 shows the simulated normalized reflected voltage of the first and second reader based on H_{11}, H_{12}, H_{21} and H_{22}. The effect of the bio-potential channel and the bio-impedance channel signals on each other is reasonably low for proper near-field data transmission.

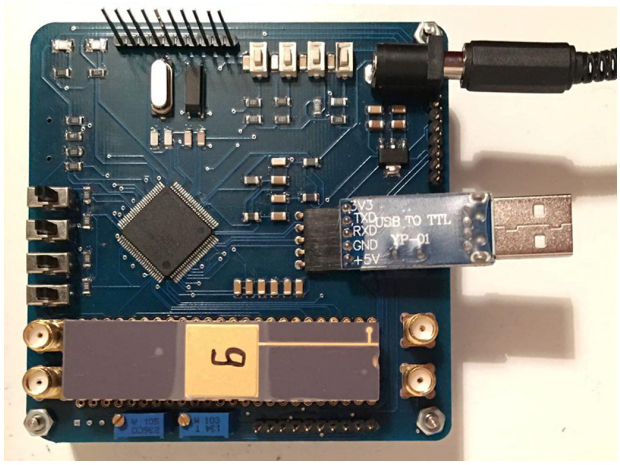

Fig. 17. ASIC test board.

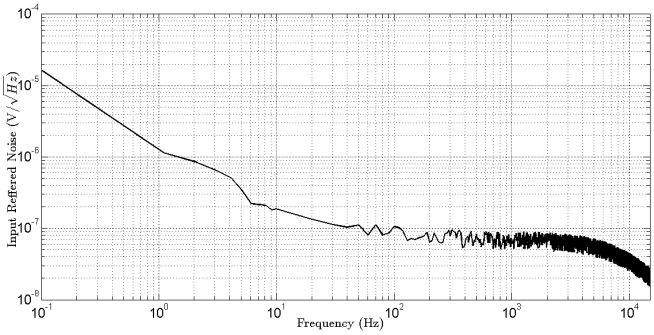

Fig. 18. Bio-potential channel input referred noise (Gain=44 dB).

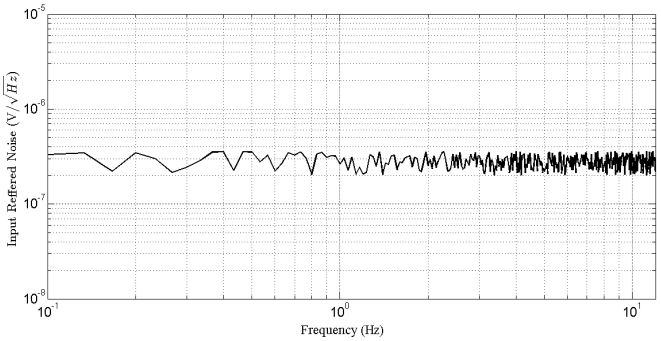

Fig. 19. Bio-impedance channel input referred noise (Gain=40 dB).

VII. Measurements

The proposed ASIC has been fabricated in a 0.18 µm HV CMOS process and occupies 2.38 mm^2 as shown in Fig. 16. Fig. 17 shows the test board for measuring the proposed system parameters and functionality by sending the various PWM signals of the proposed system via USB to the computer for reconstruction. The USB connection is for comparison of the receiver output with the on-chip data to calculate the BER of the radio link.

Without taking into account the stimulation current from the current DAC, the entire ASIC consumes only 4.2 µA from a 1 V supply. The stimulation system consumes very little power since it only stimulates the tissue occasionally and during a very short period of time (as it works at a duty cycle of appropriately 0.01%). The transmitter circuitry is passive,

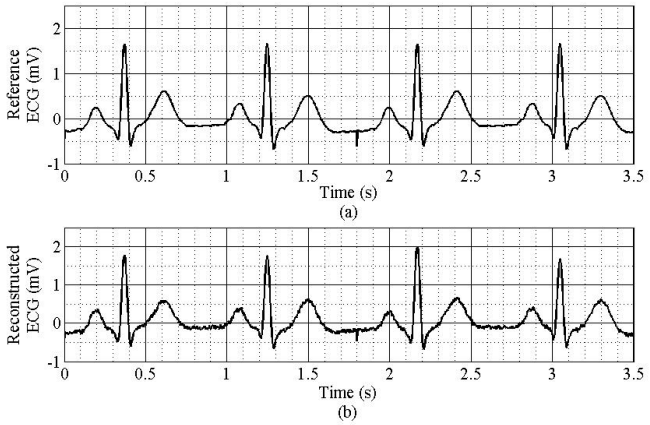

Fig. 20. Example of a measured and reconstructed ECG using the ASIC. a) The reference ECG stored in the function generator. b) The reconstructed ECG.

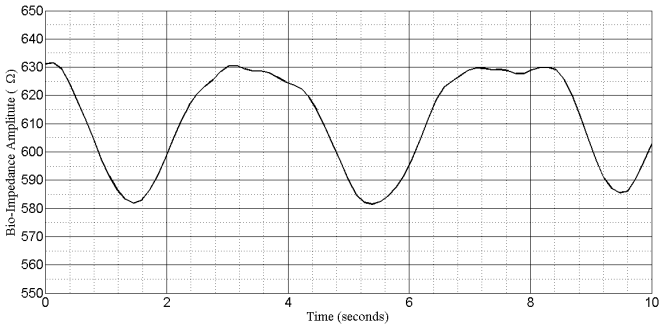

Fig. 21. Measured respiration signal on a human body using the proposed ASIC.

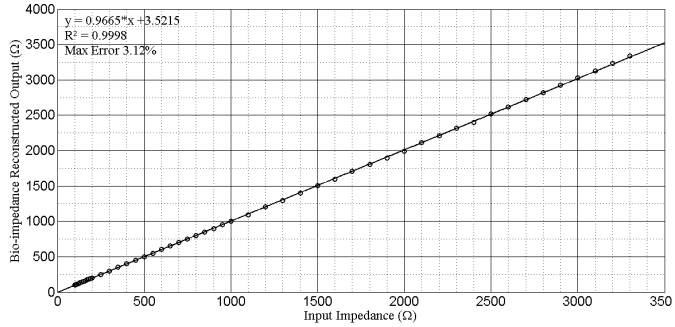

Fig. 22. Characterization of the bio-impedance channel for different resistances.

so the only power consumption stems from the switches that work at a low frequency (up to 512 kHz) and that consume very little dynamic power.

The input referred noise of the IECG readout channel measured within the signal bandwidth of 50 mHz -150 Hz is 2 μV_{rms}. The common-mode rejection ratio (CMRR) of the IA is greater than 90dB. Its power spectral density (PSD) is shown in Fig. 18. The input referred noise of the bio-impedance readout channel measured over a signal bandwidth of 0.1 Hz-10 Hz is lower than 0.7 µVrms (when the front-end gain is 40 dB). Its PSD is shown in Fig. 19. The frequencies of the multiplexer are set to 1 kHz and 3 kHz; the effective number of bits of both channels is 9.2 bits and 8.4 bits, respectively.

To illustrate the functionality of the bio-potential system, a human ECG signal (data collected from the MIT-BIH Database [24]) is put into a function generator and is

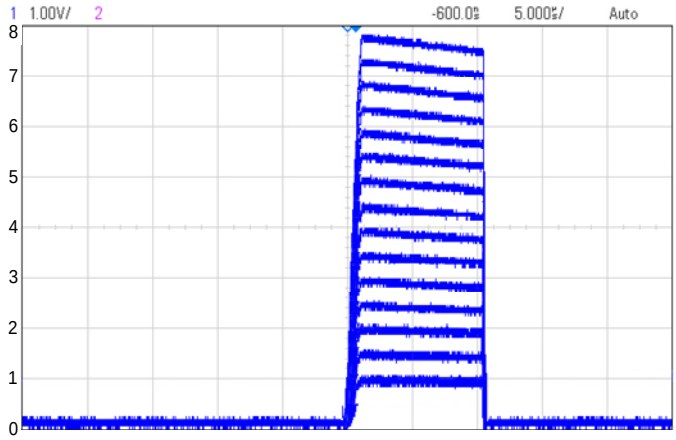

Fig. 23. High-voltage monophasic stimulator output waveform.

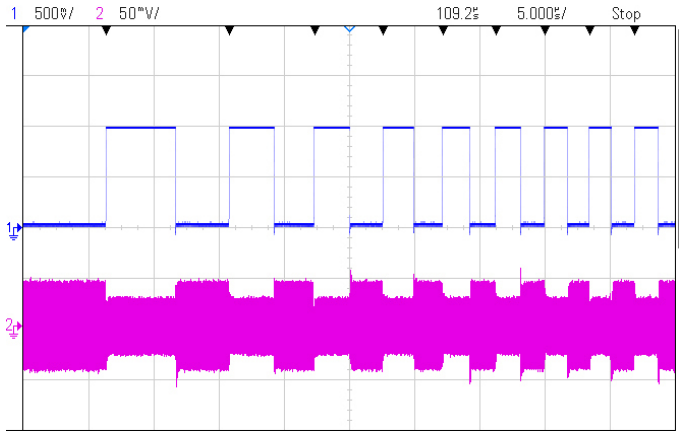

Fig. 24. Bio-potential transmitter output.

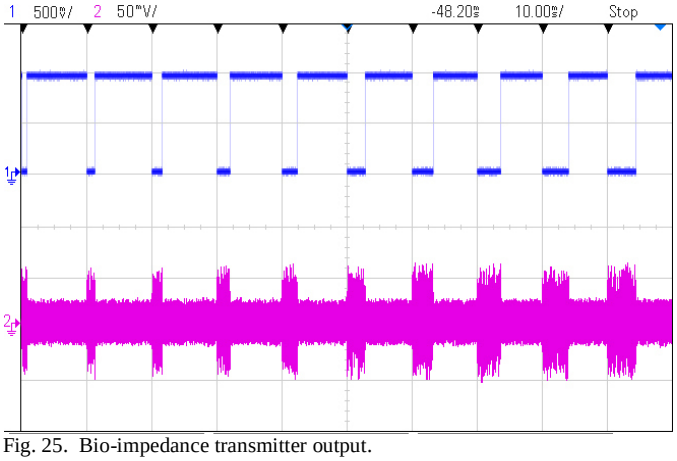

Fig. 25. Bio-impedance transmitter output.

reconstructed using the chip (Fig. 20). Furthermore, as the experiment was not conducted in a real pacemaker, usually implanted under the clavicle, either at left or at right, and its leads attached to the heart tissue, the functionality of the bio-impedance channel was validated on a human body. Thereto, four Ag/AgCl electrodes were placed on the thorax of a volunteer. Two electrodes are constructing the current loop and the other two are used for the input of the magnitude channel, revealing the respiration signal as shown in Fig. 21.

Fig. 22 shows the characterization of the bio-impedance measurement channel using different resistances. The reconstructed output of the magnitude channel shows a linear

TABLE IV
SUMMARY OF ASIC SPECIFICATION

Brief summary	1.4 mm × 1.7 mm @ 0.18 µm HV CMOS 4.2 µW Supply: 1.8 V, 1 V Core Temperature: 27°C					
	Gain (dB)	Bandwidth (Hz)	Input Referred Noise (μV_{rms})	THD	Dynamic Range	ENOB
Bio-potential channel	14-28-44	10-120	2	1%@ full swing @100 Hz	50 µV-9 mV	9.2
Bio-impedance channel	40-49-55-62	0.1-10	0.7	1%@ <1 kΩ @10 Hz	100-3.3 kΩ	-
	Min. Voltage	Max. Voltage	Osc. Frequency	Number of Bits	Settling time	Power efficiency
Stimulator	1	7.8	2 MHz	4	35 µs	55%
	Modulation	Bio-potential carrier		Bio-impedance carrier	Distance	BER
Data transmitter	OOK	13.56 MHz		21 MHz	20 mm	$<10^{-7}$

TABLE V
PERFORMANCE COMPARISON

	This Work	[1]	[2]	[3]	[6]
Technology (µm)	0.18	0.5	0.5	0.18	0.18
Supply voltage (V)	1.8 (1V core)	2.8	2	1.8	1.25
Type of sensors	IECG, Bio-Imp.	IECG	ECG, Bio-Imp.	IECG, Bio-Imp.	ECG
Number of sense channels	3	1	1	3	1
Sense resolution (ENOB)	9.2	8	10.6	9.4	8
Sense channel input referred noise (μV_{rms})	2	15	1.1	2.2	16.8
Bio-impedance measurement	Y	N	Y	Y	N
Injection current	0.5-1 µA	-	50-5.5 nA	10-40 µA	-
Bio-impedance frequency	2 kHz	-	1 kHz	2 kHz	-
Bio-impedance modulation	Semi-ramp	-	Semi-square	Square/Pseudo-sine	-
Bio-impedance accuracy (Ω_{rms})	1.35	-	12-63	0.033-0.132	-
Bio-impedance input referred noise (μV_{rms})	<0.7	-	1.7	0.46	-
Bio-impedance range (Ω)	0.1~3.3 k	-	0.1~10 k	0.1~4.4 k	-
Modulation (TX)	OOK	-	-	-	OOK
Stimulator resolution (bit)	4	3	-	-	-
DATA TX frequency (MHz)	13.56/21	-	-	-	13.56/402
Overall system size (mm)	1.4×1.7	7×7	4.6×4.5	5×5	1.9×2
Power consumption (injected current is included)	4.2 µW	8 µW	30 µW	50.6-116.6 µW	9.7 µW

transfer function for varying the resistance from 100 Ω-3.3 kΩ. The maximum error is less than 3.12%, a percentage that occurs for the higher resistance range. The accuracy of the bio-impedance channel is 1.35 Ω_{rms}.

Fig. 23 shows high-voltage monophasic stimulator output with 15 different amplitudes. Its output changes from 1 V to 7.8 V. The voltage multiplier benefits from the 2 MHz oscillator to hold the high reference voltage of the DAC at a 7.8 V level. The ASK data of the transmitter and also the transmitted data are shown in Fig. 24 and Fig. 25 for the bio-potential channel and the bio-impedance channel, respectively. The bio-potential channel and bio-impedance channel data are modulated on 13.56 MHz and 21 MHz carriers, respectively. The bit error rate of the data link extracted by comparing the radio link reconstructed output and the USB reconstructed output is better than 10^{-7} for each channel.

Table IV shows the specification summary of the proposed system at room temperature. Table V compares the performance of the proposed system with state of the art designs. Unlike other designs, the proposed ASIC provides not only the basic functions, such as bio-potential sensing, bio-impedance measurement, stimulation and data transmission, but also incorporates programmable stimulation and a novel output channel signal format that is suitable for low power transmission for biomedical applications.

VIII. FUTURE WORK

The proposed system can be extended further to feature some interesting additional functionalities, useful either for

cardiac pacemakers or other types of wearable or implantable monitoring, diagnostic or therapeutic medical devices, such as electroceuticals. Some of these extensions are discussed here.

Simultaneous wireless power transmission and data communication might help the implant to receive part or all of its power wirelessly from the external reader. This allows for reduction of the size of the (rechargeable) battery.

The bio-potential channel has the capability of changing its sampling rate. By adaptively changing the sampling rate of the ASIC and using an algorithm that changes the averaging interval in the reader, the average data rate across the wireless link is reduced, which, in turn, can lead to further reduction of the power consumption.

Thermal energy harvesting from body temperature differences is another interesting possibility to reduce the power consumption.

Currently, the size of the implant is dominated by the size of the coils in the backscatterer. To reduce the implant size, the transmitter can either use concentric coils for two channels or single-channel multiplexing of the bio-impedance and IECG signals can be applied, in a similar fashion as is currently being done for the magnitude and the phase of the bio-impedance.

IX. Conclusion

A 4.2 µA analog signal processor IC is presented for measuring bio-potentials, bio-impedance, and offering stimulation. A 0.5 µA/channel bio-potential measurement technique is presented for measuring cardiac signals making use of a voltage to frequency converter. The proposed system also consists of two channels for bio-impedance magnitude and phase measurement, which consumes only 1.55 µW, and the output of which are pulse width modulated (PWM) signals. It consumes little power by making use of pulse width modulation for transferring data via a backscattering transmitter. The proposed system is capable of measuring the bio-potential and the bio-impedance signals with 9.2 ENOB and 1.35 Ω_{rms} accuracy, respectively. Thanks to these features the proposed pacemaker system will have a smaller core and less transceiver power consumption and the entire pacemaker can last longer on its battery.

References

[1] L. S. Y. Wong, S. Hossain, A. Ta, J. Edvinsson, D. H. Rivas and H. Naas, "A very low-power CMOS mixed-signal IC for implantable pacemaker applications," in *IEEE Journal of Solid-State Circuits*, vol. 39, no. 12, pp. 2446-2456, Dec. 2004.

[2] R. F. Yazicioglu, S. Kim, T. Torfs, H. Kim and C. Van Hoof, "A 30 µ W Analog Signal Processor ASIC for Portable Biopotential Signal Monitoring," in *IEEE Journal of Solid-State Circuits*, vol. 46, no. 1, pp. 209-223, Jan. 2011.

[3] L. Yan *et al.*, "A 13 µ Analog Signal Processing IC for Accurate Recognition of Multiple Intra-Cardiac Signals," in *IEEE Transactions on Biomedical Circuits and Systems*, vol. 7, no. 6, pp. 785-795, Dec. 2013.

[4] S. Y. Lee, J. H. Hong, C. H. Hsieh, M. C. Liang and J. Y. Kung, "A Low-Power 13.56 MHz RF Front-End Circuit for Implantable Biomedical Devices," in *IEEE Transactions on Biomedical Circuits and Systems*, vol. 7, no. 3, pp. 256-265, June 2013.

[5] A. Shameli, A. Safarian, A. Rofougaran, M. Rofougaran, J. Castaneda and F. De Flaviis, "A UHF Near-Field RFID System With Fully Integrated Transponder," in *IEEE Transactions on Microwave Theory and Techniques*, vol. 56, no. 5, pp. 1267-1277, May 2008.

[6] A. L. Mansano, Y. Li, S. Bagga and W. A. Serdijn, "An Autonomous Wireless Sensor Node With Asynchronous ECG Monitoring in 0.18 µm CMOS," in *IEEE Transactions on Biomedical Circuits and Systems*, vol. 10, no. 3, pp. 602-611, June 2016.

[7] J. Xu, R. F. Yazicioglu, B. Grundlehner, P. Harpe, K. A. A. Makinwa and C. Van Hoof, "A 160µw 8-Channel Active Electrode System for EEG Monitoring," in *IEEE Transactions on Biomedical Circuits and Systems*, vol. 5, no. 6, pp. 555-567, Dec. 2011.

[8] Y. Li, A. L. Mansano, Y. Yuan, D. Zhao and W. A. Serdijn, "An ECG Recording Front-End With Continuous-Time Level-Crossing Sampling," in *IEEE Transactions on Biomedical Circuits and Systems*, vol. 8, no. 5, pp. 626-635, Oct. 2014.

[9] M. Min and T. Parve, "Improvement of Lock-in Electrical Bio-Impedance Analyzer for Implantable Medical Devices," in *IEEE Transactions on Instrumentation and Measurement*, vol. 56, no. 3, pp. 968-974, June 2007.

[10] P. Kassanos, I. F. Triantis and A. Demosthenous, "A CMOS Magnitude/Phase Measurement Chip for Impedance Spectroscopy," in *IEEE Sensors Journal*, vol. 13, no. 6, pp. 2229-2236, June 2013.

[11] R. Pelliconi, D. Iezzi, A. Baroni, M. Pasotti and P. L. Rolandi, "Power efficient charge pump in deep submicron standard CMOS technology," in *IEEE Journal of Solid-State Circuits*, vol. 38, no. 6, pp. 1068-1071, June 2003.

[12] M. Ghovanloo, "Switched-capacitor based implantable low-power wireless microstimulating systems," *2006 IEEE International Symposium on Circuits and Systems*, Island of Kos, 2006, pp. 4 pp.-.

[13] S. Y. Lee *et al.*, "A Programmable Implantable Microstimulator SoC With Wireless Telemetry: Application in Closed-Loop Endocardial Stimulation for Cardiac Pacemaker," in *IEEE Transactions on Biomedical Circuits and Systems*, vol. 5, no. 6, pp. 511-522, Dec. 2011.

[14] M. Yin and M. Ghovanloo, "Using Pulse Width Modulation for Wireless Transmission of Neural Signals in Multichannel Neural Recording Systems," in *IEEE Transactions on Neural Systems and Rehabilitation Engineering*, vol. 17, no. 4, pp. 354-363, Aug. 2009.

[15] R. A. Guinee and C. Lyden, "A novel Fourier series time function for modeling and simulation of PWM," in *IEEE Transactions on Circuits and Systems I: Regular Papers*, vol. 52, no. 11, pp. 2427-2435, Nov. 2005.

[16] R. Kubendran, S. Lee, S. Mitra and R. F. Yazicioglu, "Error Correction Algorithm for High Accuracy Bio-Impedance Measurement in Wearable Healthcare Applications," in *IEEE Transactions on Biomedical Circuits and Systems*, vol. 8, no. 2, pp. 196-205, April 2014.

[17] M. Min, T. Parve, V. Kukk and A. Kuhlberg, "An implantable analyzer of bio-impedance dynamics: mixed signal approach [telemetric monitors]," in *IEEE Transactions on Instrumentation and Measurement*, vol. 51, no. 4, pp. 674-678, Aug 2002.

[18] Medical Electrical Equipment- Part 1: General Requirements for basic Safety and Essential Performance, International Standard, IEC60601-1, 2005.

[19] S. Y. Lee, J. H. Hong, C. H. Hsieh, M. C. Liang and J. Y. Kung, "A Low-Power 13.56 MHz RF Front-End Circuit for Implantable Biomedical Devices," in *IEEE Transactions on Biomedical Circuits and Systems*, vol. 7, no. 3, pp. 256-265, June 2013.

[20] Y. Rezaeiyan, M. Zamani, O. Shoaei, and W. A. Serdijn, "A 0.5 µA/Channel front-end for implantable and external ambulatory ECG recorders," *Microelectronics Journal*, vol. 74, pp. 79-85, April 2018.

[21] M. Zamani, Y. Rezaeiyan, O. Shoaei and W. A. Serdijn, "A 1.55 µW Bio-Impedance Measurement System for Implantable Cardiac Pacemakers in 0.18 µm CMOS," in *IEEE Transactions on Biomedical Circuits and Systems*, vol. 12, no. 1, pp. 211-221, Feb. 2018.

[22] X. Zhang and Y. Lian, "A 300-mV 220-nW Event-Driven ADC With Real-Time QRS Detection for Wearable ECG Sensors," in *IEEE Transactions on Biomedical Circuits and Systems*, vol. 8, no. 6, pp. 834-843, Dec. 2014.

[23] H. Kim *et al.*, "A Configurable and Low-Power Mixed Signal SoC for Portable ECG Monitoring Applications," in *IEEE Transactions on Biomedical Circuits and Systems*, vol. 8, no. 2, pp. 257-267, April 2014.

[24] http://ecg.mit.edu/

[25] Charles J. Love, *Cardiac Pacemaker and Defibrillators*. Landes Bioscience, Inc.; 2nd edition, 2006.

[26] N. Van Helleputte *et al.*, "A 345 µW Multi-Sensor Biomedical SoC With Bio-Impedance, 3-Channel ECG, Motion Artifact Reduction, and Integrated DSP," in *IEEE Journal of Solid-State Circuits*, vol. 50, no. 1, pp. 230-244, Jan. 2015.
[27] L. Yan *et al.*, "A 3.9mW 25-electrode reconfigured thoracic impedance/ECG SoC with body-channel transponder," *2010 IEEE International Solid-State Circuits Conference - (ISSCC)*, San Francisco, CA, 2010, pp. 490-491.
[28] H. Ko, T. Lee, J. H. Kim, J. a. Park and J. P. Kim, "Ultralow-Power Bioimpedance IC With Intermediate Frequency Shifting Chopper," in *IEEE Transactions on Circuits and Systems II: Express Briefs*, vol. 63, no. 3, pp. 259-263, March 2016.
[29] S. A. P. Haddad, R. P. M. Houben and W. A. Serdijn, "The evolution of pacemakers," in *IEEE Engineering in Medicine and Biology Magazine*, vol. 25, no. 3, pp. 38-48, May-June 2006.
[30] S. Y. Lee, C. J. Cheng and M. C. Liang, "A Low-Power Bidirectional Telemetry Device With a Near-Field Charging Feature for a Cardiac Microstimulator," in *IEEE Transactions on Biomedical Circuits and Systems*, vol. 5, no. 4, pp. 357-367, Aug. 2011.
[31] M. Min and T. Parve, "Thoracic bioimpedance as a basis for pacing control," Ann. New York Acad. Sci., vol. 873, no. 1, pp. 155–166, 1999.
[32] M. Min, A. Kink, and T. Parve, "Rate adaptive pacemaker using impedance measurements and stroke volume calculations," US Patent 6,975,903, Dec 13, 2005.
[33] J. G. Webster, Design of Cardiac Pacemaker, New York, NY, USA: IEEE, 1995.

Yasser Rezaeiyan was born in Khomein, Iran, in 1988. He received the B.Sc. degree in Electrical Engineering from Shahid Chamran University of Ahwaz in 2010 and the M.Sc. degree in Electrical Engineering from Sharif University of Technology in 2012.

He is currently working towards the Ph.D. degree in the Section Biomedical Circuit and System Design at the Faculty of Electrical and Computer Engineering, University of Tehran, Tehran, Iran. His research interests include ultra-low-power analog integrated circuit and system design for biomedical applications. Currently he is with the Section Bioelectronics at TU Delft as a guest researcher.

Milad Zamani (S'16) was born in Babol, Iran, in 1988. He received the B.Sc. degree in Electrical Engineering from University of Tehran, Iran, in 2010 and the M.Sc. degree in Electrical Engineering from Sharif University of Technology, Iran, in 2012.

He is currently pursuing the Ph.D. degree in the Section Biomedical Circuit and System Design at the Faculty of Electrical and Computer Engineering, University of Tehran, Tehran, Iran. His current research interests include low power analog integrated circuits and systems design for biomedical applications. Currently he is with the Section Bioelectronics at TU Delft as a guest researcher.

Omid Shoaei (M'96) received the B.Sc. and M.Sc. degrees from University of Tehran, Iran, in 1986 and 1989, respectively, and the Ph.D. degree from Carleton University, Ottawa, Ont., Canada, in 1996, all in Electrical Engineering.

From 1994 to 1995 he was with BNR/NORTEL, Ottawa, as a Ph.D. intern student, working on high-speed delta-sigma modulators. In 1995 he was with Philsar Electronics Inc., Ottawa, working on the design of a bandpass delta-sigma data converter.

From December 1995 to February 2000, he was a Member of Technical Staff with Bell Labs, Lucent Technologies, Allentown, PA, where he was involved in the design of mixed analog/digital integrated circuits for LAN and Fast Ethernet systems. From February 2000 to March 2003, he was with Valence Semiconductor Inc. design center in Dubai, UAE, as director of the mixed-signal group, where he developed voice codec and SLIC, and also several data converter IP's for 802.11a and HomePlug V.2. Later from 2004 to 2007 he developed a pair of 24-bit audio delta-sigma ADC/DAC and a 12-bit 100MHz pipeline ADC. From 2008 to 2012, he was with Qualcomm in San Diego, where he led the development of two audio codec chipsets that so far have been shipped in millions to tier one cell phone OEMs.

From 1998 to 2008, Dr. Shoaei was also an associate professor at the Univ. of Tehran, where he has been affiliated with since Feb. 2012.

He has received 3 U.S. patents, and is the author or co-author of more than 170 international and national journal and conference publications. His research interests include biomedical integrated circuits and systems, analog-to-digital converters, and precision analog/mixed-signal circuits and systems.

Wouter A. Serdijn (M'98, SM'08, F'11) was born in Zoetermeer ('Sweet Lake City'), the Netherlands, in 1966. He received the M.Sc. (cum laude) and Ph.D. degrees from Delft University of Technology, Delft, The Netherlands, in 1989 and 1994, respectively. Currently, he is a full professor in bioelectronics at Delft University of Technology, where he heads the Section Bioelectronics, and a visiting honorary professor at University College London, in the Analog and Biomedical Electronics group.

His research interests include integrated biomedical circuits and systems for biosignal conditioning and detection, neuroprosthetics, transcutaneous wireless communication, power management and energy harvesting as applied in, e.g., hearing instruments, cardiac pacemakers, cochlear implants, neurostimulators, portable, wearable, implantable and injectable medical devices and electroceuticals.

He is co-editor and co-author of 10 books, 8 book chapters, 3 patents and more than 300 scientific publications and presentations. He teaches Circuit Theory, Analog Integrated Circuit Design, Analog CMOS Filter Design, Active Implantable Biomedical Microsystems and Bioelectronics. He

received the Electrical Engineering Best Teacher Award in 2001, in 2004 and in 2015.

He has served, a.o., as General Co-Chair for IEEE ISCAS 2015 and for IEEE BioCAS 2013, Technical Program Chair for IEEE BioCAS 2010 and for IEEE ISCAS 2010, 2012 and 2014, as a member of the Board of Governors (BoG) of the IEEE Circuits and Systems Society (2006—2011), as chair of the Analog Signal Processing Technical Committee of the IEEE Circuits and Systems society, and as Editor-in-Chief for IEEE Transactions on Circuits and Systems—I: Regular Papers (2010—2011). Currently, he is the chair of the Steering Committee and an Associate Editor of the IEEE Transactions on Biomedical Circuits and Systems (T-BioCAS).

Wouter A. Serdijn is an IEEE Fellow, an IEEE Distinguished Lecturer and a mentor of the IEEE. In 2016, he received the IEEE Circuits and Systems Meritorious Service Award.